Segregation of Nociceptive and Non-Nociceptive Networks in the Squirrel Monkey Somatosensory Thalamus

A. VANIA APKARIAN,[1] TING SHI,[1] JOHANNES BRÜGGEMANN,[1] AND LEVON R. AIRAPETIAN[2]
[1]*Department of Neurosurgery, SUNY Upstate Medical University, Syracuse, New York 13210; and* [2]*Yerevan Physics Institute, Yerevan 375049, Republic of Armenia*

Received 13 September 1999; accepted in final form 21 March 2000

Apkarian, A. Vania, Ting Shi, Johannes Brüggemann, and Levon R. Airapetian. Segregation of nociceptive and non-nociceptive networks in the squirrel monkey somatosensory thalamus. *J Neurophysiol* 84: 484–494, 2000. The somatosensory thalamus (here we examine neurons in the caudal cutaneous portion of ventral posterior lateral nucleus, VPL) is composed of a somatotopic arrangement of anteroposteriorly oriented rods. Each rod is a collection of neurons with homogeneous properties that relay sensory information to specific cortical columns. We developed a multi-electrode recording technique, using fixed-geometry four-tip electrodes that allow simultaneous recordings from small populations of neurons (4–11), in a $\sim 150 \times 150 \times 150$ μm^3 volume of brain tissue (i.e., the approximate diameter of rods) and study of their spatiotemporal interactions. Due to the fixed geometry of the four-tip electrodes, the relative locations of these neurons can be determined, and due to the simultaneity of the recordings, their spike-timing coordination can be calculated. With this method, we demonstrate the existence of two distinct functional networks: nociceptive and non-nociceptive networks. The population dynamics of these two types of networks are different: cross-correlations in each type of network were different in direction and strength, were a function of the distance between neurons, had an opponent organization for nociceptive networks and a non-opponent organization for non-nociceptive networks, and rapidly changed under different stimulus conditions independent of changes in firing rates. A simple neural network model mimicked these physiological findings, demonstrating the necessity of inhibitory interneurons and different amounts of afferent input synchronization. Based on these results, we conclude that the somatosensory thalamus is composed of two modules, nociceptive and non-nociceptive rods, and that the response dynamics differences between these modules are due to spatiotemporal differences of their afferent inputs.

INTRODUCTION

From a single-unit recording point of view, the thalamus is generally regarded as faithfully transmitting incoming inputs to the cortex. A variety of electrophysiological studies have asserted this viewpoint at least for the three primary sensory nuclei of the thalamus: somatosensory, visual, and auditory (Jones 1985). For example, the properties of neurons in the somatosensory thalamus, such as receptive field size, position, and modality specificity, reflect incoming medial lemniscal properties, which were thought to be relayed with little transformation to the cortex (Poggio and Mountcastle 1963). However, it is also clear that the thalamus plays a complex role in the processing of sensory information with different states of sleep, vigilance, and maybe even memory consolidation (Steriade 1999).

Single-unit recording techniques are certainly suitable to characterize the response properties of individual neurons, and by correlating these physiological data with anatomic and behavioral data, a vast amount of knowledge has been gained about the organization of the nervous system. To date, nociceptive representation in the primate thalamus has only been studied using single electrodes with single- or multi-unit recording techniques. Nociceptive cells have been described in a number of thalamic nuclei (Apkarian and Shi 1994; Bushnell et al. 1993; Casey and Morrow 1983; Dostrovsky and Craig 1996; Kenshalo et al. 1980; Lenz et al. 1993; Willis 1985). In this study, we concentrate on nociceptive representation in the lateral somatosensory region [cutaneous caudal portion of ventral posterior lateral nucleus (VPL)]. In the monkey VPL, most nociceptive cells respond convergently to innocuous and noxious stimuli and are described randomly intermingled with non-nociceptive cells (e.g., Apkarian and Shi 1994). These responses have been characterized based on changes in the mean firing rate of individual cells. Recent studies, however, indicate that spike-timing changes, i.e., changes in the coordination of spikes across neurons, may be another mechanism for coding afferent inputs. Populational studies in the cortex indicate that besides relying on a mean rate of neuronal firings, coordination in relative timing of action potentials across neurons may be a fundamental principle of information coding (deCharms and Merzenich 1996; Gray et al. 1989; Singer and Gray 1995). Single-unit recordings cannot detect such coordination changes. The spatial and temporal interactions between neighboring and distant neurons (populational codes) can only be determined by simultaneous recordings from groups of neurons (e.g., Nicolelis et al. 1993). In this study, we reexamine the role of the somatosensory thalamus in nociceptive information coding when spiking activity of small groups of neighboring neurons are examined simultaneously.

Given the strong bidirectional connectivity between the cortex and the thalamus and given that most sensory inputs (except the olfactory) are relayed through the thalamus, what is the role of the thalamus in the spike-timing-based population codes revealed in the cortex? We examine this question using

Address for reprint requests: A. V. Apkarian, Dept. of Neurosurgery, Research Laboratories, WKH 3118, SUNY Upstate Medical University, 766 Irving Ave., Syracuse, NY 13210 (E-mail: apkarian@mail.upstate.edu).

The costs of publication of this article were defrayed in part by the payment of page charges. The article must therefore be hereby marked "*advertisement*" in accordance with 18 U.S.C. Section 1734 solely to indicate this fact.

our new population recording technique. The lateral somatosensory thalamic populational codes are examined when the skin is stimulated with innocuous and noxious stimuli. Spike-timing coordination changes are determined as a function of stimulus and as a function of distance between neurons.

This work is in partial fulfillment of the PhD dissertation requirements for T. Shi.

METHODS

Neuronal population activity was recorded using four-tip tungsten electrodes in the somatosensory thalamus of five squirrel monkeys. The monkeys were chronically implanted with a recording chamber, and once every 1–2 wk were anesthetized with 0.5–1.2% halothane, in 1/3 N_2O and 2/3 O_2, and used for recordings. In each monkey during the first recording session, single tungsten electrode recordings were made to establish the boundaries of VPL. Subsequent recordings used the four-tip electrodes, targeting neuronal groups in VPL. The housing, care, and surgical procedures followed the institutional guidelines established by the Committee for the Humane Use of Animals. At a given recording site, multi-unit activity collected from each of the tips was recorded and displayed on a personal computer. The receptive field of the units was determined on-line based on the multi-unit responses. Innocuous and noxious stimuli were then applied within this receptive field. The collected data were clustered off-line to individual neuronal activity, and their responses, coordination, and locations in space relative to the recording tips were calculated.

Initial surgery

The surgery for chamber implantation was done under sterile conditions. Each of the animals was pretreated with dexamethasone (0.25 mg/kg im) and antibiotics (Rocephin 75 mg/kg im) prior to surgery. Anesthesia was induced with ketamine (30 mg/kg im) and continued with a mixture of 0.5–1.2% halothane, 1/3 N_2O and 2/3 O_2 during surgery. The animals were intubated and given lactated Ringer solution intravenously. Expired CO_2, oxygen saturation, and heart rate were monitored non-invasively and maintained within physiologic range. Body core temperature was maintained within 36.5–38°C by an electrical blanket. The skull was opened to access VPL, leaving the dura intact. A stainless steel recording chamber was implanted over the opening and attached to the occipital skull with screws and dental cement. The chamber was filled with saline and Neosporin and sealed with a screw. Following surgery, the animals were administered antibiotics for 3 days and checked for normal recovery. The chamber was cleaned every week. The first recording session was 2–3 wk after implantation.

Recording and stimulation

The same anesthesia used for the initial surgery was used during recording sessions. The anesthetic level was kept at a level where withdrawal responses to noxious stimuli were suppressed. Vital signs were monitored as in the preceding text. The animal was intubated and breathed spontaneously.

The animal was initially placed in a stereotactic frame. After the head was immobilized by attaching a holder to the skull, the stereotactic head frame was removed. Single tungsten microelectrodes were used to map and electrophysiologically identify VPL. Subsequent recordings were performed with four-tip electrodes. The neuronal activity was collected using a multi-channel amplifier (Model CDA-100, Micro Probe), and processed using commercial software running on a personal computer (DataWave Technologies, Longmont, CO). The data-sampling rate was 20 kHz for each channel. Spike discrimination windows were set at the same threshold for each of the channels, and the noise level was adjusted to the same by controlling the gain of the amplifiers. The time for acquiring a spike was set 0.5 ms prior to and 1.0 ms after the time when the rise phase of a spike exceeded the discrimination threshold. If a spike was detected on one channel, all other channels would be triggered and potentials on all channels collected simultaneously. The neuronal activity including spike shapes, on-line peristimulus-time histograms (PSTH), and the stimulus analog curves were displayed on a monitor and stored for off-line analyses. The analog signals were also stored on videotape using a digital system (Vetter, Rebersburg, PA).

Somatic mechanical response properties and receptive fields of the main units on each channel were determined on-line. Mechanical stimuli included brush (bristles 5–10 g, 2–3 Hz), touch (50–100 g, 2–3 Hz), tap (with a smooth probe, 100–200 g, 2–3 Hz), pressure (large forceps or weights, 100–200 g on a 5–10 mm diameter area), pinch (serrated clamp, 600–900 g on a 5-mm-diam area), and deep tissue squeeze. The pinch and squeeze stimuli were painful when applied to the experimenter. During data analysis, all stimuli were catalogued into four modalities: spontaneous activity, brush (including brush, touch, and tap), pressure, and pinch.

Four-tip electrode

The fixed-geometry four-tip electrodes (custom made by FHC, Bowdoinham, ME) synchronously monitored activity across all tips. Since each triggered event was recorded from all four tips, off-line analysis based on the shapes of the action potentials on all four tips enabled identifying single-unit activity, a procedure identical to the one first introduced for tetrodes (Wilson and McNaughton 1993). We optimized the electrode tip geometry to enable recording from as many distinct thalamic neurons as possible while monitoring individual spikes by all four tips. Thus these electrodes combine the advantages of single-cell recordings (large signal-to-noise ratio of tungsten electrodes) with that of tetrodes (a fourfold increase in the confidence that a unit is properly classified as coming from the same neuron). The electrode tips make up a tetrahedron with the electrodes being 115 μm apart horizontally and electrodes 1 and 3 being 100 μm shorter than the other two. These electrodes enable examining the spatiotemporal properties of small groups of neighboring neurons.

Clustering individual neurons

The multiple units recorded on each channel were sorted and clustered with Autocut (DataWave). The amplitudes and time to peak on each channel were used as parameters to differentiate spike shapes. The joint scatter of these parameters, for each pair of channels, clusters the spikes into different neurons (spike generation points). Clusters were differentiated using 2.25 SD distance from the center of a given cluster as the minimum cutoff between clusters. The clusters cut automatically were slightly modified by the experimenter.

Classification of response properties

Response types were determined both subjectively (on-line) and by measuring the mean change in the rate of unit responses (off-line). A given unit was classified as responsive to a specific stimulus only if its mean firing rate changed significantly (t-test, $P < 0.05$) and by $\geq$30%. Neurons were classified as low threshold (LT) when the increase in activity was not different between innocuous and noxious stimulation, as wide dynamic range (WDR) when noxious stimulation elicited a higher neuronal activity as compared with innocuous pressure, and as nociceptive specific when only noxious stimulus intensities lead to increased neuronal activity (see Apkarian and Shi 1994).

During on-line monitoring of multi-unit activity, if units on any electrode tip responded to a noxious stimulus, the recording site was defined as *nocisite*. Sites where on-line multi-unit activity did not show nociceptive responses were defined as *non-nocisites*. This clas-

sification was compared with the responses of the neurons after being separated off-line.

Locating spike generation sites

Distance calculations between neurons relative to the electrode tips were based on the average spike amplitudes observed on each tip. The decay rate of spike amplitude as a function of distance was determined in single-electrode recordings (Fig. 1). The experimentally measured decay rates were smoothed and the variance in fitting the data with various power rules was calculated. The minimum variance resulted from a Euclidean distance rule ($P = 2$ in Fig. 1*C*). This dependence was determined in dorsoventral penetrations using single electrodes (Fig. 1, *A* and *B*). The same rule was assumed to apply to the action potential decay in the other two spatial dimensions (mediolateral and anteroposterior) since most VPL cells (projecting neurons and interneurons) are spherical (Shi and Apkarian 1995; Turner et al. 1997; Williams et al. 1996). Therefore we assume that an action potential gives rise to a three-dimensional bell shaped potential curve, the peak of which we define as the spike generation point. This rule is then applied to localize spike generation points in the four-tip recordings.

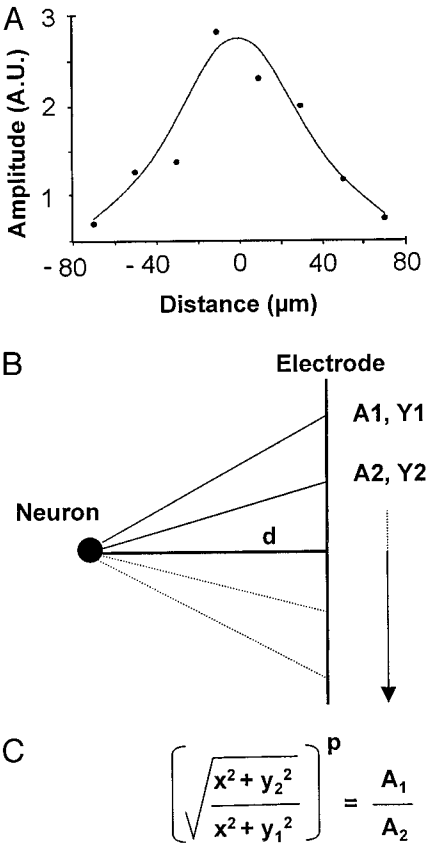

FIG. 1. Determination of the minimal distance between a single-electrode tip and a recorded single neuron. *A*: change of action potential size of a single neuron during a dorsoventral penetration of a single electrode through ventral posterior lateral nucleus (VPL). The Gaussian fit is shown as a continuous curve. The depth where the maximal amplitude was recorded was defined as "zero". *B*: schematic of the relationship between dorsoventral depth of the electrode tip in relation to the position of a single neuron. The bold vertical line represents the electrode; the arrow indicates the direction the electrode was moved. *C*: the equation used to calculate the minimal distance between electrode tip and a single neuron. A_1, size of the action potential at the first depth y_1; A_2, size of the action potential at another depth y_2; *d*, minimal distance between electrode tip and neuron (bold horizontal line in *B*), exponent of the relationship between relative action potential size (in arbitrary units, A. U. in *A*), and the distance (in μm in *A*) between electrode tip and neuron; *x*, initial guess value to solve the equation.

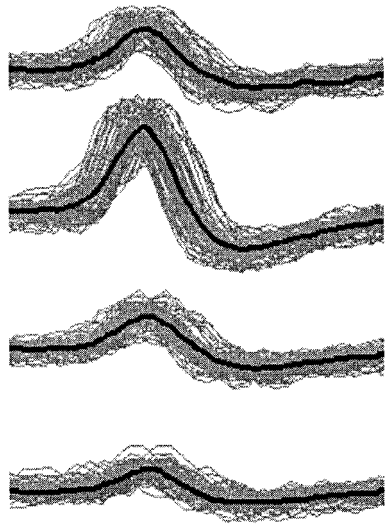

FIG. 2. Recordings of a single neuron as monitored from all 4 tips of the electrode. Gray: superimposed single action potentials; black lines: average amplitudes. Total duration of the displayed action potentials is 1.5 ms.

Because the impedances of the four tips are similar and also signal levels of the four channels are normalized by adjusting background noise levels, a neuron's (n_i) average spike amplitudes on the four channels (as shown in Fig. 2), d_1, d_2, d_3, or d_4, can be used to calculate its distance from each electrode, by solving the 4×4 matrix derived directly from the Euclidean distance rule

$$d_1 = (Xn_i - Xe_1)^2 + (Yn_i - Ye_1)^2 + (Zn_i - Ze_1)^2$$

$$d_2 = (Xn_i - Xe_2)^2 + (Yn_i - Ye_2)^2 + (Zn_i - Ze_2)^2$$

$$d_3 = (Xn_i - Xe_3)^2 + (Yn_i - Ye_3)^2 + (Zn_i - Ze_3)^2$$

$$d_4 = (Xn_i - Xe_4)^2 + (Yn_i - Ye_4)^2 + (Zn_i - Ze_4)^2$$

where Xn_i, Yn_i, and Zn_i are the coordinates of the position of neuron n_i in the cube formed by the four electrode tips, (Xe_1, Ye_1, Ze_1) define the coordinates of electrode tip 1, the other tip coordinates are defined similarly. An example of the measured positions of 10 neurons at one recording site is shown in Fig. 3*A*. This calculation of the position of a given neuron relative to the four electrode tips is based on the basic assumption that the size and shape of the action potentials recorded from each tip remains constant.

Figure 2 also shows the variability in the size of the action potential measured on each channel. This translates into a positional variability, which we estimate to be $\sim$10 μm in all three dimensions. Therefore any given spike generation point has a 5–10% jitter relative to the dimensions of the four-tip electrode.

Cross-correlations

The cross-correlations were calculated with a window width of 200 ms, a bin size of 1 ms, and smoothed with a Gaussian function (Abeles 1982). Statistically significant cross-correlation peaks or valleys were defined as three or more bins exceeding 2 SD from the mean spike count and lasting for at least four bins within the first 30 ms. Cross-correlation strength was calculated by measuring the area of the peak or valley above the mean count, multiplied by bin size, and divided by the total number of spikes. The latter expresses the cross-correlation strength in extra spikes observed above the mean number of spikes. The negative cross-correlation strengths are underestimated with this procedure; however, we did not manipulate these measures any further to present the most conservative estimates of cross-correlation strengths.

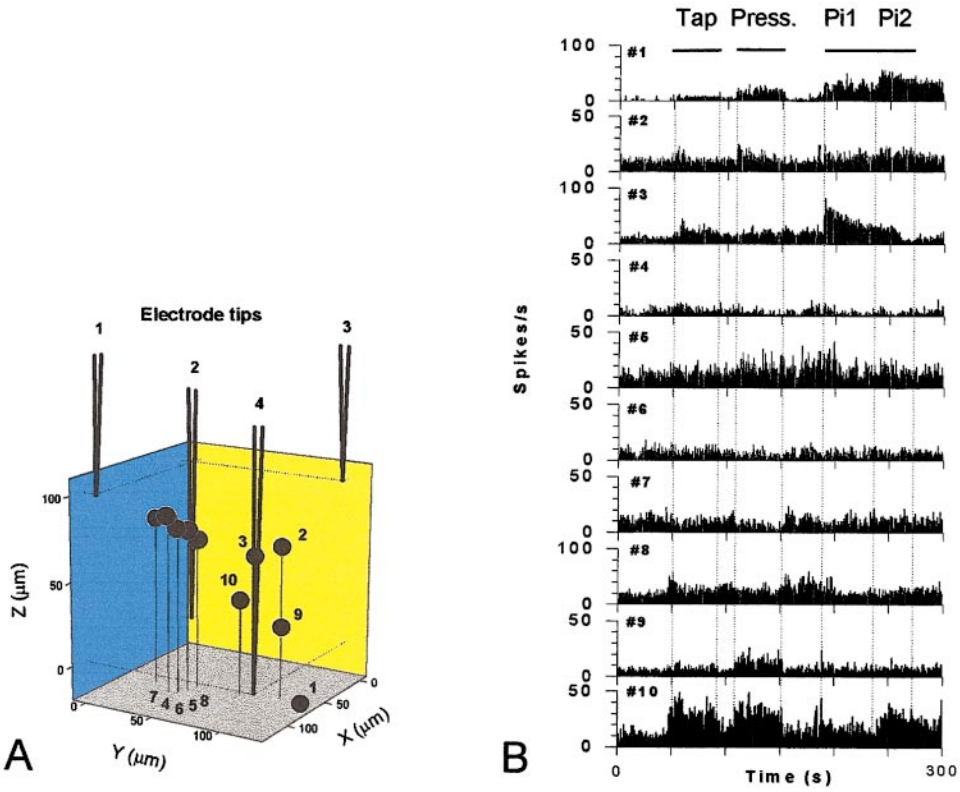

FIG. 3. *A*: 3-dimensional structure of the 4-tip electrode and the calculated locations of 10 neurons of a cluster found in VPL. The distance between adjacent electrodes is 115 μm, and tips 1 and 3 are 100 μm shorter than tips 2 and 4. The distances between the neurons ranged from 17 to 108 μm. *B*: firing rates as a function of somatic innocuous and noxious stimuli for a 10-neuron cluster found in a 150 × 150 × 150 μm^3 volume of VPL tissue. The somatic mechanical stimuli applied to the skin are indicated relative to the histograms of firing rates. Tap and pressure (press.) are innocuous stimuli. Pinch 1 (Pi1, 600 g over a 2 mm^2 area) and pinch 2 (Pi2, 900 g over 2 mm^2 area) are increasing intensity noxious stimuli. Four of the 10 neurons respond to the noxious stimuli, thus this recording site was classified as a nocisite.

Neural network model

A four-element neural network model was developed to help explain our physiological findings. The model consisted of two inhibitory interneurons (i_1, i_2) and two projecting neurons (p_1, p_2). There is no direct connection between the projecting neurons. The inhibitory interneurons are driven by the projecting neurons through excitatory synapses and in turn are negatively connected to the opposite projecting neuron. All afferent inputs are excitatory and impinge on all four neural elements. Synaptic connections are defined by time varying probabilities. Asynchronous inputs are defined as spikes arriving independently and with a random distribution on all four neural elements. Synchronous inputs are events that arrive in fixed time relationship to each other (with or without delays), with a random interval between events. The cross-correlations between p_1 and p_2 were calculated as a function of firing rate and quality of afferent inputs (nonsynchronized, or synchronized). Details of the simulations are posted on our web site (http://alpha.nmrlab.hscsyr.edu/pain/).

Histology

The animals were perfused with 4% paraformaldehyde in 0.1 M phosphate buffer (pH 7.2). Fifty-micrometer frontal sections of the brain were mounted, and alternating sections were Nissl stained and stained for cytochrome oxidase to identify recording tracts. We did not make electrolytic lesions in these animals because these were surviving animals and were used in multiple recording sessions over a time period of several months and because VPL was mapped and physiologically identified with a single electrode in each experiment before a four-tip electrode was used.

RESULTS

Most recording sites were ascertained to be in VPL by histology (Fig. 4). However, because the recordings were done in a chronic preparation over a period of months, not all tracks could be histologically identified. Altogether 34 penetrations with four-tip electrodes were performed, and 15 tracts were recovered in the histological sections. The locations of the tracks inside VPL (13 tracks) matched the receptive field properties of the individual neurons. The majority of the recovered tracks (13/15) penetrated VPL (see Fig. 4, *top*). In the experiment where two tracks were outside (lateral) of VPL, the protocol report indicates one penetration with no receptive fields and another one where visual inputs were recorded. Therefore we assume that most of the recordings were done from the caudal cutaneous portion of VPL based on stereotaxic coordinates, neuronal responses, and the topographic arrangement of body representation.

At 10 recording sites the distance between the studied neurons, averaged for 308 pairs of neurons was 54 ± 29 (mean ± SD) μm. One hundred and twenty four neurons were isolated from 17 recording sites. At each recording site clusters of 4–11 (7 ± 2, mean ± SD) neurons were identified. Distances between neurons in histological sections of the squirrel monkey VPL were found to range between 10 and 150 μm, and there were 20–40 neurons in a 115 × 115 × 100 μm^3 volume of VPL tissue. Therefore we estimate that 1/4–1/2 of the neurons embedded between the four electrode tips were identified as active neurons and studied. Figure 4, *bottom*, is an example of the reconstruction of part of a recording site in a 50-μm-thick coronal section, showing the tracks of two of the four tips. Thirteen somata can be seen. Because our electrode tips are ~100 μm apart, this would result in an estimate of ~26 neurons at this recording site, which compared with our mean number of physiologically identified neurons again shows that ~1/4 of the local neurons were studied.

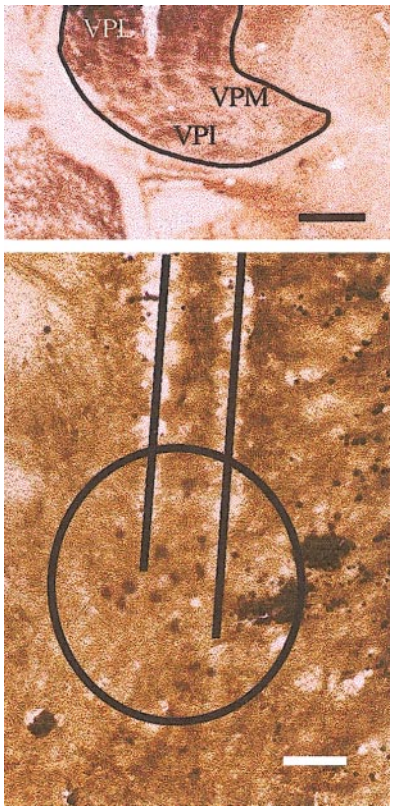

FIG. 4. CO-stained coronal sections (50 μm) through a squirrel monkey somatosensory thalamus at 2 different magnifications (*top bar*: 1 mm; *bottom bar*: 100 μm). *Top*: the black line delineates the borders of the ventral posterior complex. The 2 parallel lines (*bottom*) indicate the tracks of 2 tips of a 4-tip electrode. The circle indicates the "sphere" from which we estimate we record from. The intensity of the color of somata inside the circle has been enhanced for better visibility. VPI, ventroinferior posterior nucleus; VPM, ventromedial posterior nucleus.

Single-unit properties

The receptive fields of the neurons recorded at 16 sites were cutaneous and deep at one recording site. At all 17 sites receptive fields of neurons were contralateral and near each other and limited to one extremity or to the tail.

Eighty-three neurons were clustered from 11 nocisites and 41 neurons were clustered from 6 non-nocisites. The pooled prevalence of nociceptive neurons was 0.16 across all recording sites. The variability of the prevalence of nociceptive neurons among the 17 sites, relative to an hypothesis of a common prevalence, produced a deviance (G_o^2, with 16 df) of 24.9, suggesting heterogeneity in the distribution of nociceptive cells. All recording sites defined on-line as nocisites indeed contained nociceptive neurons, while recording sites defined on-line as non-nocisites contained neurons responsive only to innocuous stimuli. Within nocisites, 25% (21 cells) were classified as LT type and 24% (20 cells) as nociceptive. At non-nocisites, 51% (21 cells) were classified as LT and none as nociceptive. The remaining neurons responded either inconsistently (~30%) or not at all (the remaining 18%) to repeated stimulation. The mean firing rates of the nociceptive neurons during spontaneous activity, brush, pressure, and pinch were 10.2 ± 8.9, 12.3 ± 10.8, 19.9 ± 14.4, and 26.5 ± 16.4 spikes/s, respectively.

Figure 3*B* shows mean firing rates at a nocisite composed of a 10-neuron cluster, when tap, pressure, and two intensities of pinch were applied to the same body part. *Neurons 1*, *3*, *8*, and *10* responded to tap; *neurons 1*, *2*, *3*, *5*, and *8–10* responded to pressure; and *neurons 1*, *2*, *3*, and *10* responded to pinch stimuli. At this site three neurons were nociceptive, four non-nociceptive, and three did not respond to any of these stimuli. Therefore the responses, when based on mean firing rates, illustrate the intermingling of nociceptive neurons with other neurons.

Cross-correlations

To examine the spike-timing relationship between neurons, cross-correlations between neuron pairs identified in single recording sites were examined. Figure 5 shows cross-correlations at one site for four stimulus conditions. Cross-correlations are shown only for *neurons 1* and *2* with the rest of the population for the cluster whose firing rates are shown in Fig. 3. Figure 5 illustrates that most cross-correlations with large positive peaks are unidirectional (span one side or the other of *time 0*). There are also a large number of negative valleys, most of which are of short-duration and close to *time 0*, and there are dramatic changes in the cross-correlations for different stimu-

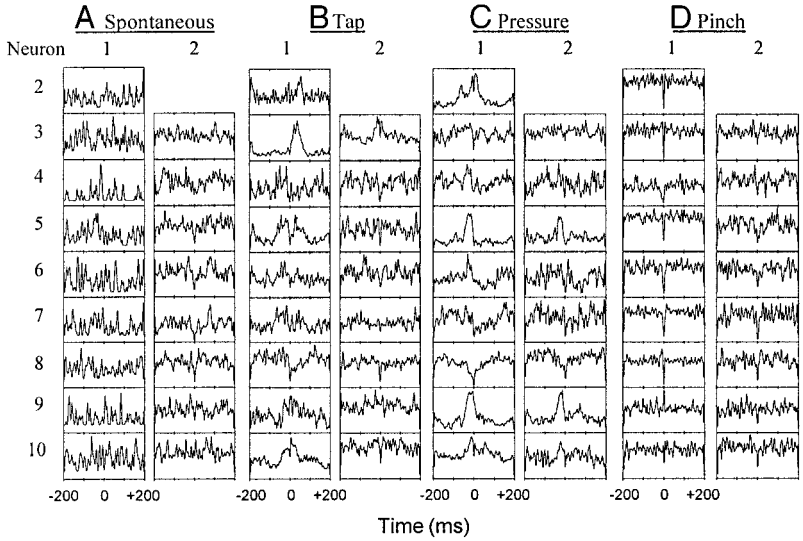

FIG. 5. Spike-timing coordination between neurons seems stimulus specific. Cross-correlations are shown for four stimulus conditions for the neuron cluster shown in Fig. 3. Spike timings of *neurons 1* and *2* with the others are illustrated in the paired cross-correlations. Note that many cross-correlations differ between stimulus conditions.

lus conditions. In this example, cross-correlations are significantly changed between *neurons 1* and *3*, *1* and *5*, *1* and *9*, *1* and *10* and *2* and *3*, *2* and *5*, *2* and *9* across the four stimulus conditions. Also, most cross-correlations between *neuron 1* and the rest turn negative during pinch (Fig. 5*D*). Moreover there is no clear relationship between firing rates and cross-correlations. Generally stimulus related firing rate changes were not predictive of cross-correlation changes at noci- and at non-nocisites. Figure 6 illustrates the relationship between cross-correlations ("connectivity") and mean firing rates, as a function of stimulus, for the same 10 neuron cluster shown in Fig. 3*A*. There are no discernible connectivity relationships between the cells responsive or non-responsive to the stimuli. Also the changes in connectivity from one stimulus to the next (tap vs. pinch) reorganizes the network connectivity but again with no clear relationship to the neurons that respond to the stimuli.

The properties of spike timings were distinct between noci- and non-nocisites. The percentage of neuron pairs with significant cross-correlations was dependent on the type of recording site and the polarity of the correlations. There were more positively correlated pairs at non-nocisites (38.9 ± 20.6%, n = 6 sites) than at nocisites (27.6 ± 11.7%, n = 11) and more negatively correlated pairs at nocisites (14.1 ± 10.1%) than at non-nocisites (4.9 ± 6.7%; 2-way ANOVA, for recording sites $F = 33.1$ $P < 0.0001$ and for correlation polarities $F = 55.5$ $P < 0.0001$). The cross-correlation incidences were also stimulus modality dependent: At non-nocisites, the number of positive cross-correlations increased during brush (from 11 ± 6.3/site during spontaneous activity to 17.7 ± 9.1/site; Kruskal-Wallis 1-way ANOVA, $P < 0.01$). At nocisites, the number of negative cross-correlations increased during pinch (from 4.2 ± 2.6/site during spontaneous activity to 6.2 ± 4.3/site; Kruskal-Wallis 1-way ANOVA, $P < 0.05$). Positive cross-correlations were much stronger (0.20 ± 0.29, n = 467) than the negative ones (−0.07 ± 0.05, n = 197). Moreover at nocisites the time delay to reach the peak or valley of the cross-correlations was a function of stimulus and of polarity. The time delays to the peak of positive cross-correlations for spontaneous activity, brush, pressure, and pinch stimuli, respectively, were 8.69 ± 7.76, 10.18 ± 8.67, 9.67 ± 8.3, and 7.22 ± 6.32 ms (n = 121, 147, 116, and 83), and the time delays to the valley of negative cross-correlations were 3.85 ± 6.85, 4.07 ± 6.66, 2.62 ± 4.66, and 1.45 ± 1.23 ms (n = 47, 44, 53, and 53; 2-way ANOVA, for polarity $F = 91.09$, $P < 0.0001$ and for stimulus modalities $F = 3.41$, $P < 0.05$). These significant differences in correlation properties between sites indicate that the non-noci- and nocisites are segregated far better by spike-timing relationships between neurons than by the mean firing rates of individual neurons, which indicated only borderline differences in the prevalence of nociceptive neurons across recording sites.

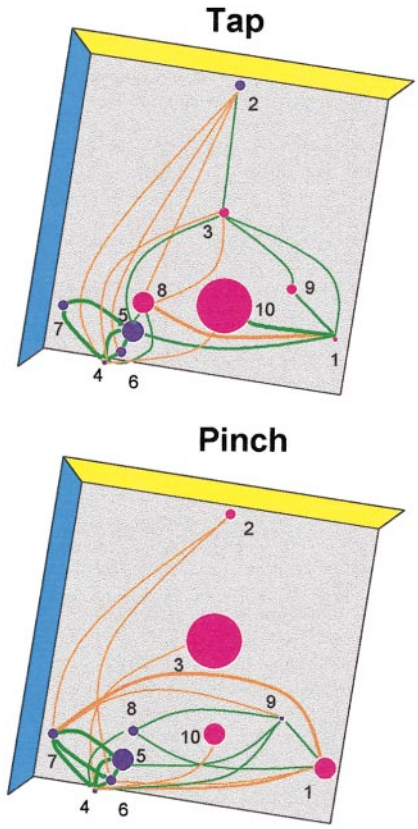

FIG. 6. Location, responsiveness, and connectivity of the cluster of 10 neurons described in Fig. 3*A*. The 3-dimentional view has been changed to better illustrate the changes in responsiveness and connectivity. The colors of the dots indicate responsiveness (red) or unresponsiveness (blue) to tap (*top*) or pinch (*bottom*). The colors of the lines indicate significant excitatory (green), or inhibitory (red) cross-correlations between the neurons. The sizes of the dots indicate the mean firing rate during the stimuli.

Connectivity as a function of distance

The four-tip electrodes enable calculating distances between neurons at a given recording site (Fig. 3*A*), and for the same neurons, the presence of statistically significant cross-correlations and their strengths also can be determined. We combined these measures to generate spatial maps of spike-timing relationships for the population, separated by groupings (noci- vs. non-nocisites) and stimulus conditions. Both the strength (Fig. 7, *A* and *B*) and the incidence (Fig. 7, *C* and *D*) of cross-correlations as a function of distance indicate the presence of an opponent organization of spike timings at nocisites and a non-opponent organization at non-nocisites. At nocisites, strong positive correlations occur at short distances (65% of the positive cross-correlations are for neuron pairs with <40 μm separations); and negative cross-correlations rarely occur (<2%) between nearby neurons (<30 μm) ($\chi^2 = 191$, $P < 0.0001$). Most negative cross-correlations are seen between neuron pairs separated by 30–120 μm. These spatial properties of spike timings at noci- and at non-nocisites undergo subtle complex changes with different stimuli. In one case, this stimulus-dependent change seems readily interpretable. At the non-nocisites, the incidence of positive cross-correlations for nearby neurons (<40 μm) decreases during the pinch stimulus (in comparison to the spontaneous activity and longer distances, Fisher's exact $P = 0.052$), consistent with the independence assumption between neuronal activity at these sites and noxious stimuli.

Minimal neural network model

These experimental results show changes in spike-timing relationships between neurons for different sensory stimuli. What types of mechanisms are necessary to bring about such

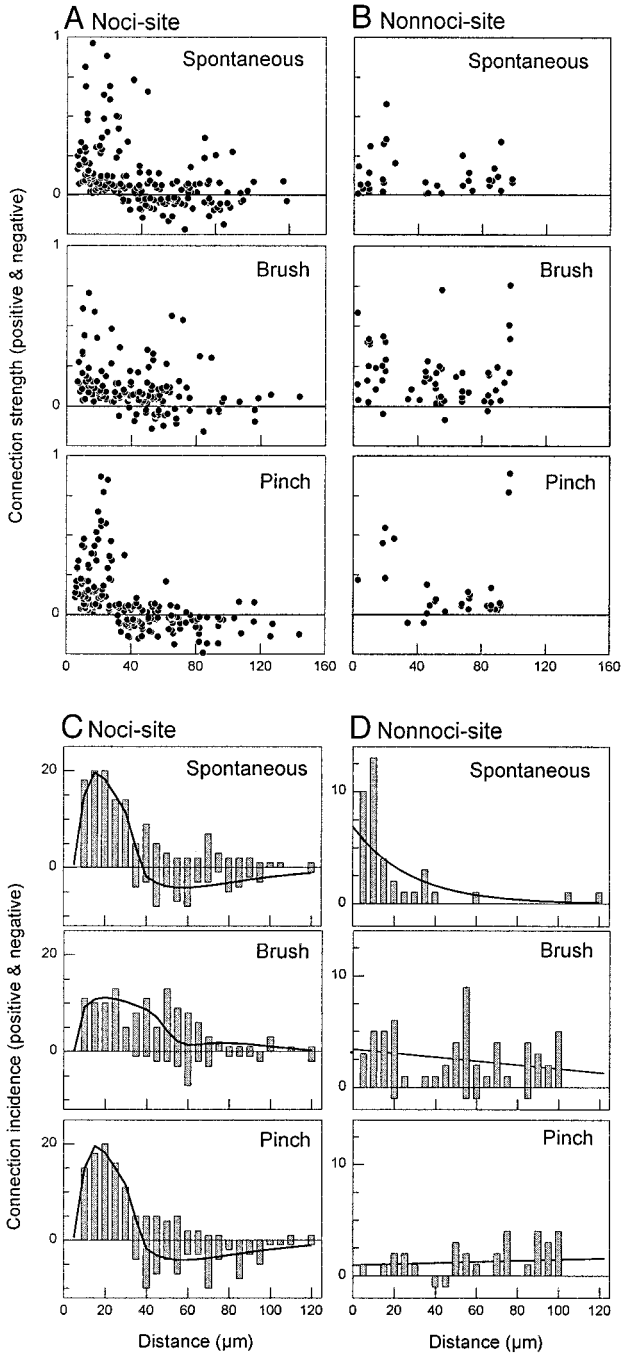

FIG. 7. Spatial maps of spike timings are dependent on recording site and stimulus modality. Spatial maps of spike timings are generated by combining cross-correlation strength and distance (*A* and *B*) and cross-correlation incidence and distance (*C* and *D*) for all pairs of neurons with statistically significantly strong cross-correlations. In *C*, the positive and negative incidence distributions were separately fitted with Weibull functions. —, the difference between the positive and negative fits. The incidence map for the non-nocisite in the absence of stimulation (*D*, spontaneous) was fitted with a single exponential, during innocuous and noxious stimulation the maps were fitted to lines (—).

timing changes? Moreover why do we observe such a prominence of negatively correlated neuronal activity in the thalamus, when these are rarely seen in the cortex? Figure 8*A* shows a simulated neural network, which captures the major timing relationships that we observe and illustrates our conceptual model. The model indicates the presence of inhibitory interneurons (i_1, i_2) between projecting cells (p_1, p_2) that are appropriately distant from each other. The inhibitory interneurons are necessary for nocisites when the pair of neurons are distant from each other. The cross-correlations between p_1 and p_2, for the four-element network is shown for non-synchronized afferent inputs (unconnected arrows in model; result shown in Fig. 8*B*) and for synchronized inputs (connected arrows in model; results shown in Fig. 8, *C–E*). As the non-synchronized inputs increase, the mean firing rates of p_1 and p_2 increase and the negative symmetrical cross-correlation becomes stronger and observable due to the presence of i_1 and i_2 (Fig. 8*B*). Most negative cross-correlations that we observe physiologically are of this type, mainly seen at nocisites during pinch. For a fixed mean firing rate, increasing the strength of the synchronized

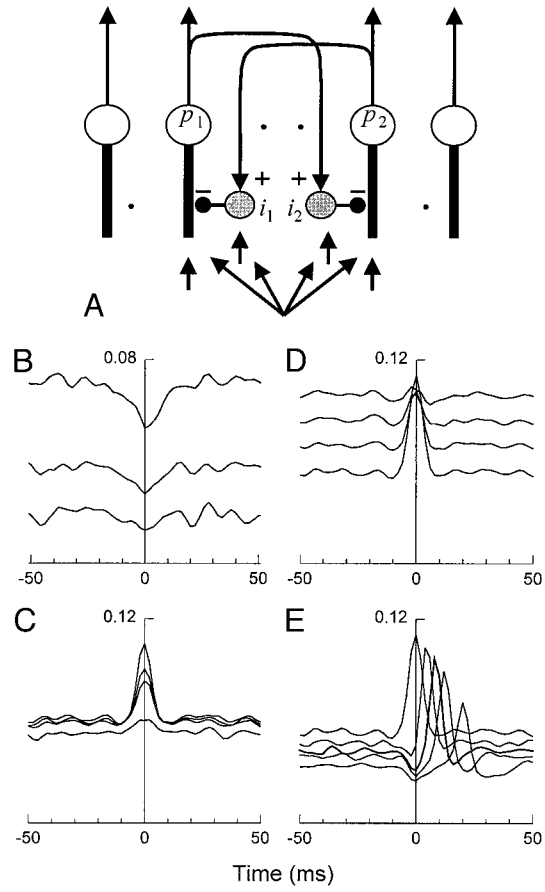

FIG. 8. *A*: a 4-element network model where different inputs give rise to the cross-correlations illustrated below. Small dots symbolize appropriate distant neurons intermingled with the 4-element network, (i_1, i_2), inhibitory interneurons; (p_1, p_2) projecting cells that are appropriately distant from each other; (unconnected arrows in model, *B*), the cross-correlations between p_1 and p_2, for non-synchronized afferent inputs; (connected arrows in model, *C–E*) for synchronized inputs. *B*: as the non-synchronized inputs increase, the mean firing rate increases and the negative cross-correlation becomes stronger and observable. *C*: for a fixed mean firing rate, increasing the strength of the synchronized input increases the peak of the positive cross-correlation. *D*: for fixed-strength synchronized inputs, as the amount of non-synchronized input is increased, the mean firing rate increases and the positive peak of the cross-correlation decreases. *E*: if the synchronized input arrives at p_1 and p_2 with the same delay, the positive cross-correlation peak is symmetrical around *time 0.* Different delays between the inputs to p_1 and p_2 results in shifted positive cross-correlation peaks. In *B–D,* the *x* axis is time in ms, the *y* axis is probability of spike generation. The details of these simulations are posted on our web site (http://alpha.nmrlab.hscsyr.edu/pain/)

input (relative to the non-synchronized input) increases the peak of the positive cross-correlation (Fig. 8*C*). For fixed-strength synchronized inputs, as the amount of non-synchronized input is increased the mean firing rate increases and the positive peak of the cross-correlation decreases (Fig. 8*D*). If the synchronized input arrives at p_1 and p_2 with the same delay, the positive cross-correlation peak is symmetrical around *time 0*. Different delays between the inputs to p_1 and p_2 result in shifted positive cross-correlation peaks (Fig. 8*E*). Therefore depending on the amount of synchronized inputs and their delay properties, one obtains positive cross-correlations that are either symmetrical or unilateral. The unilateral cross-correlation implies a unidirectional information flow between two units that are not directly connected with each other. The cross-correlations demonstrated in Fig. 8, *B–E* are all seen in our experimental data. This network therefore demonstrates spike-timing coordination changes that span the main changes we see physiologically. Importantly, this is achieved without changing the local synaptic connectivity of the network and only manipulating the amount of synchronous versus asynchronous afferent inputs.

DISCUSSION

We recorded simultaneously from members of groups of thalamic neurons located in small, contiguous neighborhoods. The properties of these neurons were characterized in the traditional single-electrode/single-cell recording method and by examining the spatiotemporal interactions between neurons in any given neighborhood. Mechanical innocuous and noxious stimuli segregate these neurons into nociceptive and non-nociceptive cells and segregate the groups of cells into noci- and non-nocisites. While the prevalence of nociceptive neurons in VPL was in the same range as reported in single-cell recording studies (Apkarian and Shi 1994), the changes in firing rates during stimulation were not predictive of changes in the cross-correlations of pairs of neurons. The results of the present study demonstrate that the neuronal interactions at non-nocisites are distinct from those found at nocisites with respect to several aspects: non-nocisites had more positive cross-correlations, while nocisites had more inhibitory cross-correlations (which are seldom seen in the cortex); the incidence of cross-correlations was stimulus dependent; and at nocisites indications for surround inhibition were observed, and there was no evidence for such an organization at non-nocisites.

Single-unit properties

We estimate that ~18% of the neurons were unresponsive. We do not think that this is due to missing receptive fields because at any given recording site most of the body of the animal was investigated with innocuous stimuli, and the multi-unit responses on each of the four tips of the electrode were determined. However, we could have missed some nociceptive neurons because noxious stimuli were not applied as systematically as innocuous ones. This is not likely, however, because in a previous study (Apkarian and Shi 1994), using single-electrode/single-unit recording techniques the incidence of nociceptive neurons was 10% in VPL, and in the present study, it was 25% at nocisites, indicating that with our four-tip electrode technique, nociceptive neurons can be detected quite efficiently. In addition, we did not study neurons with very low ongoing activity, and neurons with inconsistent responses were only studied in the correlation analysis.

The properties of VPL neurons recorded in the present study are similar to those reported in single-electrode recordings in firing rates, receptive fields, somatotopy, and response properties (for references, see Apkarian and Shi 1994). Although the receptive fields of individual neurons were not determined for every cell, on-line monitoring showed that these neurons had the characteristic receptive fields of VPL neurons. Almost all nociceptive cells had responses to innocuous stimuli as well (i.e., they would be classified as WDR type), except one, which only responded to pinch (nociceptive specific type). In our single-electrode recording study of VPL cells, all except two nociceptive cells were of WDR type (Apkarian and Shi 1994). The overall incidence of nociceptive cells in the current study was 16% (20/124), which is slightly higher than in our single-electrode recording study (9.4% or 19/203, χ^2 test, $P > 0.1$). Since all nociceptive neurons were found at the nocisites, the percentage (24%) is even higher at nocisites. These observations and the homogeneity test imply that the nociceptive cells are grouped in bunches in VPL and that recording sites containing such neurons are physiologically and functionally distinct from those containing only non-nociceptive neurons. In addition, nociceptive neurons have been repeatedly described intermingled with neurons responsive selectively to innocuous stimuli (Apkarian and Shi 1994; Bushnell et al. 1993; Casey and Morrow 1983; Lenz et al. 1993; Willis 1985). The latter is consistent with our observation that at nocisites, 25% of the cells respond to innocuous stimuli only.

The segregation of nociceptive neurons is in agreement with the patchy spinothalamic terminals (which is thought to be the most important pathway to convey nociceptive information) found in anatomic studies (Apkarian and Hodge 1989; Berkley 1980; Hodge and Apkarian 1990; Rausell et al. 1992; Shi et al. 1993). It is also possible that the nocisites correspond to the "matrix" domain in VPL since the matrix domain is suggested to be more specific to spinothalamic inputs (Rausell et al. 1992). Our results do not support this hypothesis since the matrix region is a cell-poor region, mostly devoid of GABAergic cells (Rausell and Jones 1991). Our data show a very similar rate of incidence of cells per site between noci- and non-nocisites (mean 7.5 and 6.8, respectively; χ^2 test $P > 0.9$), and the neural network model implies the necessity of GABAergic inhibitory interneurons at nocisites, although this conclusion is tempered by the lack of histological evidence regarding the exact locations of our recordings in VPL in relation to the matrix domain. In fact Rausell et al. (1992) state that the spinothalamic terminations in VPL only "tend to be concentrated" in the matrix region, and our physiological sampling does not show this tendency. A more compelling demonstration of the segregation of spinothalamic and medial lemniscal inputs in the macaque VPL was shown by Ralston and Ralston (1994). They demonstrated that the spinothalamic inputs contact relay neurons forming primarily simple axodendritic synapses, and only 15% of these terminations are on GABAergic interneurons. In contrast, medial lemniscal inputs are mediated through complex synaptic structures (triads and glomeruli, 85% of the medial-lemniscal terminals), within these structures they make direct contacts with relay neurons (54%) and indirect contacts through GABAergic structures

(46%). Therefore the medial lemniscal and spinothalamic inputs have distinct synaptic signatures in VPL.

Populational properties

To our knowledge, this is the first description of the local connectivity properties of groups of neurons studied in the CNS. A long list of connectivity measures distinguishes between noci- and non-nocisites. Therefore noci- and non-nocisites must be regarded as distinct functional entities within VPL.

Both positive and negative cross-correlations were seen in the monkey VPL, and these were related to the type of site and stimulus modality. In VPL of rat and cat, cross-correlations between neurons recorded with a single microelectrode are also reported to be positive, negative, unilateral, and symmetrical (Alloway et al. 1995). Alloway et al. report that 35–40% of pairs of nearby neurons showed positive correlations during innocuous stimulation. This incidence is very similar to our results for innocuous stimuli (positive correlations to brush at non-nocisites were 32% and at nocisites, 48%).

In the current study, most cross-correlations with large positive peaks were unidirectional (span one side or the other of *time 0*). There are also a large number of negative valleys, most of which are of short-duration and close to *time 0*. Both properties seem unique to the thalamus because in the cortex the majority of cross-correlations exhibit positive, bidirectional peaks, implying coordinated spike timings (deCharms and Merzenich 1996; Gray et al. 1989; Singer and Gray 1995; Vaadia et al. 1995). Thus the occurrence of inhibitory cross-correlations appears to be a specific feature of the thalamus and specific for nocisites.

Both in the cortex and at non-nocisites in VPL, the density of inhibitory GABAergic interneurons are similar (15–25%), yet in both places negative cross-correlations are rarely observed. This, as demonstrated in our model, must be a reflection of the strength of the inhibitory synapses, the rate of ongoing activity and extent of synchronicity of the afferent inputs. In contrast, at nocisites even during spontaneous activity, we observe a large number of negative correlations. Therefore at nocisites, the synaptic strengths of inhibitory interneurons must be stronger than at non-nocisites. Two types of GABAergic interneurons have been described in the ventrobasal complex of the cat (Meng et al. 1996). We speculate that these two types may correspond to the two classes of GABAergic neurons implied by our results. If we generalize to assume that nocisites reflect spinothalamic inputs and non-nocisites reflect medial lemniscal inputs (Apkarian 1995; Hodge and Apkarian 1990; Willis 1985), then the relay cells at nocisites receive primarily direct excitatory spinothalamic inputs while the cells at non-nocisites receive medial lemniscal inputs that are damped presynaptically through interactions with GABAergic structures. Since, as the neural network model illustrates, the type of afferent input can mask the interneuronal connectivity in the cross-correlation calculation, the extensive presynaptic modulation that medial lemniscal inputs undergo may explain the correlation properties of the non-nocisites. On the other hand, the more direct excitatory spinothalamic inputs to both relay cells and interneurons imply that the circuitry of the model presented may better correspond to the connectivity of nocisites. It should be emphasized that the details of the local circuitry among afferent inputs, relay cells, interneurons and thalamic reticular inhibitory inputs, and cortical back projections remain for the most part unknown. Also, at non-nocisites the innocuous stimuli, we used to study the populational properties were very simple. To reveal the full dynamics of non-nocisites, we need to explore a larger array of cutaneous patterns.

Dependence of connectivity on interneuronal distances

The plots of connection strength and connection incidence as a function of the distances between neurons imply a three-dimensional radial symmetry regarding local connectivity rules. To our knowledge, this is the first physiologic determination of local connectivity in the CNS. The results in general confirm an idea first proposed by Sholl (Sholl 1956; Sholl and Uttley 1953) that connection strength from any given neuron should decrease exponentially by distance. Sholl proposed the idea based on the anatomy of dendritic branching patterns in the cortex, where he actually calculates the distance decay rate for stellate cells. We observe an exponential decay in VPL at non-nocisites during spontaneous activity in accordance to Sholl's rule. Similar but more complex dependences are seen for nocisites and for various stimulus conditions. That these connectivity rules are dynamically modified by the stimulus conditions reinforces the notion that spike-timing coordination across neurons may be a fundamental principle of information coding in the thalamus and more specifically in coding innocuous and noxious somatic inputs, as already proposed for the cortex (Abeles et al. 1993, 1995; deCharms and Merzenich 1996; Gray et al. 1989; Singer and Gray 1995; Vaadia et al. 1995).

At non-nocisites, the spatial connectivity dramatically reorganizes between spontaneous activity and brush. Such reorganization of local connectivity must be the mechanism by which cutaneous receptive fields dynamically shift in time, forming a spatiotemporal distributed representation of the whiskers in the thalamus (Faggin et al. 1997; Nicolelis et al. 1995) (multielectrode recordings in the whisker region of the thalamus and cortex where population dynamics is examined for cells separated from each other by millimeters). At nocisites, we observe an opponent organization of connectivity. To our knowledge, this is the first demonstration of a center-surround organization at the level of a central neuronal network and the first observation of a center surround organization in the nociceptive system. If this organization also holds true for thermal stimuli, then it can be the mechanism that gives rise to the large cortical inhibitions we have recently described for painful stimuli applied to a very small part of the body (Apkarian et al. 2000). This may also be the mechanism by which the thermal grill illusion comes about because we have recently proposed that this illusion can be explained by lateral inhibition (Brüggemann and Apkarian 1999).

Implications of the model

The architecture of the neural network model we propose is identical to the local connectivity proposed for lateral thalamic nuclei many years ago based on anatomic studies (see Fig. 20 in Szentagothai and Arbib 1975). According to the simple neural model we developed, positive cross-correlation

strengths depend on the afferent synaptic strengths and the relative proportion of synchronized and non-synchronized inputs. It needs to be emphasized that these network properties are between pairs of model neurons that do not have direct synaptic connectivity between them. Most likely differences in the local anatomic connectivity would partially explain the opponent versus non-opponent organization of noci- and non-nocisites, although this remains to be studied more carefully. It is reasonable to assume that the afferent pathway to the nocisites is the spinothalamic tract, while the primary afferent pathway for non-nocisites is the dorsal column pathway (Apkarian 1995; Hodge and Apkarian 1990; Willis 1985). Therefore the opponent versus non-opponent organization of the noci- and non-noci-networks is attributed to differences in the spatiotemporal properties of the two pathways, in terms of the amount of synchronized and non-synchronized inputs relative to the synaptic strengths between projecting cells and interneurons. This organization of the somatosensory thalamus must also depend on the thalamo-cortico-thalamic loops as previously demonstrated for pairs of neurons in the visual thalamus (Sillitto et al. 1994).

Our results indicate that non-nocisites and nocisites in the somatosensory thalamus are segregated, i.e., we are recording from different functional entities. The size of the volume of tissue we are recording from and the similarity of the incidence of neurons at both types of sites leads us to the conclusion that we are recording from thalamic rods. This then implies the existence of two types of rods with distinct inputs: nocirods with dominant input from the spinothalamic pathway supplying asynchronous inputs during noxious stimuli and non-nocirods with dominant input from the dorsal column system supplying relatively more synchronous inputs. The three-dimensional structure of these two different functional networks is not known yet, i.e., whether they are elongated, continuous aggregates, or spherical and intermingled, which remains to be determined.

We thank Drs. D. R. Chialvo, S. A. Khan, B. Motter, and D. Pelli for comments on the manuscript.

This work was supported by the Department of Neurosurgery, SUNY Health Science Center, and the National Institute of Mental Health. J. Brüggemann was funded by Fogarty and Alexander von Humboldt fellowships.

REFERENCES

ABELES M. Quantification, smoothing, and confidence limits for single-units' histograms. *J Neurosci Methods* 5: 317–325, 1982.

ABELES M, BERGMAN H, GAT I, MEILIJSON I, SEIDEMANN E, TISHBY N, AND VAADIA E. Cortical activity flips among quasi-stationary states. *Proc Natl Acad Sci USA* 92: 8616–8620, 1995.

ABELES M, VAADIA E, BERGMAN H, PRUT Y, HAALMAN I, AND SLOVIN H. Dynamics of neuronal interactions in the frontal cortex of behaving monkeys. *Concepts Neurosci* 4: 131–158, 1993.

ALLOWAY KD, JOHNSON MJ, AND AARON GB. A comparative analysis of coordinated neuronal activity in the thalamic ventrobasal complex of rats and cats. *Brain Res* 691: 46–56, 1995.

APKARIAN AV. Thalamic anatomy and physiology of pain perception: connectivity, somato-visceral convergence and spatio-temporal dynamics of nociceptive information coding. In: *Forebrain Areas Involved in Pain Processing*, edited by Besson JM, Guilbaud G, and Ollat H. Paris: John Libbey Eurotext, 1995, p. 93–118.

APKARIAN AV, GELNAR PA, KRAUSS BR, AND SZEVERENYI NM, Cortical responses to thermal pain depend on stimulus size: a functional MRI study. *J. Neurophysiol.* 83: 3113–3122, 2000.

APKARIAN AV AND HODGE CJ. Primate spinothalamic pathways. I. A quantitative study of the cells of origin of the spinothalamic pathway. *J Comp Neurol* 288: 493–511, 1989.

APKARIAN AV AND SHI T. Squirrel monkey lateral thalamus. I. Somatic nociresponsive neurons and their relation to spinothalamic terminals. *J Neurosci* 14: 6779–6795, 1994.

BERKLEY KJ. Spatial relationships between the terminations of somatic sensory and motor pathways in the rostral brainstem of cats and monkeys. I. Ascending somatic sensory inputs to lateral diencephalon. *J Comp Neurol* 193: 283–317, 1980.

BRÜGGEMANN J AND APKARIAN AV. The thermal grill illusion can be explained by lateral inhibition (Abstract). *18th Annual Scientific Meeting of the American Pain Society*, 1999, p. 91.

BUSHNELL MC, DUNCAN GH, AND TREMBLAY N. Thalamic VPM nucleus in the behaving monkey. I. Multimodal and discriminative properties of thermosensitive neurons. *J Neurophysiol* 69: 739–752, 1993.

CASEY KL AND MORROW TJ. Ventral posterior thalamic neurons differentially responsive to noxious stimulation of the awake monkey. *Science* 221: 675–677, 1983.

DECHARMS RC AND MERZENICH MM. Primary cortical representation of sounds by the coordination of action-potential timing. *Nature* 381: 610–613, 1996.

DOSTROVSKY JO AND CRAIG AD. Cooling-specific spinothalamic neurons in the monkey. *J Neurophysiol* 76: 3656–3665, 1996.

FAGGIN BM, NGUYTEN KT, AND NICOLELIS MAL. Immediate and simultaneous sensory reorganization at cortical and subcortical levels of the somatosensory system. *Proc Natl Acad Sci USA* 94: 9428–9433, 1997.

GRAY CM, KONIG P, ENGEL AK, AND SINGER W. Oscillatory responses in cat visual cortex exhibit inter-columnar synchronization which reflects global stimulus properties. *Nature* 338: 334–337, 1989.

HODGE CJ AND APKARIAN AV. The spinothalamic tract. *Crit Rev Neurobiol* 5: 363–397, 1990.

JONES EG. *The Thalamus*. New York: Plenum, 1985.

KENSHALO DR JR, GIESLER GJ JR, LEONARD RB, AND WILLIS WD. Responses of neurons in primate ventral posterior lateral nucleus to noxious stimuli. *J Neurophysiol* 43: 1594–614, 1980.

LENZ FA, SEIKE M, LIN YC, BAKER FH, ROWLAND LH, GRACELY RH, AND RICHARDSON RT. Neurons in the area of human thalamic nucleus ventralis caudalis respond to painful heat stimuli. *Brain Res* 623: 235–240, 1993.

MENG X-W, OHARA PT, AND RALSTON HJ III. Nitric oxide synthase immunoreactivity distingueshes a sub-polulation of GABA-immunoreactive neurons in the ventrobasal complex of the cat. *Brain Res* 728: 111–115.

NICOLELIS MA, BACCALA LA, LIN RC, AND CHAPIN JK. Sensorimotor encoding by synchronous neural ensemble activity at multiple levels of the somatosensory system. *Science* 268: 1353–1358, 1995.

NICOLELIS MA, LIN RC, WOODWARD DJ, AND CHAPIN JK. Dynamic and distributed properties of many-neuron ensembles in the ventral posterior medial thalamus of awake rats. *Proc Natl Acad Sci USA* 90: 2212–2216, 1993.

POGGIO GF AND MOUNTCASTLE VB. The functional properties of ventrobasal thalamic neurons studied in unanesthetized monkeys. *J Neurophysiol* 26: 775–806, 1963.

RALSTON HJ III, AND RALSTON DD. Medial lemiscal and spinal projections to the macaque thalamus: an electron microscopic study of differing GABAergic circuitry serving thalamic somatosensory mechanisms. *J Neurosci* 14: 2485–2502, 1994.

RAUSELL E, BAE CS, VINUELA A, HUNTLEY GW, AND JONES EG. Calbindin and parvalbumin cells in monkey VPL thalamic nucleus: distribution, laminar cortical projections, and relations to spinothalamic terminations. *J Neurosci* 12: 4088–4111, 1992.

RAUSELL E AND JONES EG. Histochemical and immunocytochemical compartments of the thalamic VPM nucleus in monkeys and their relationship to the representational map. *J Neurosci* 11: 210–225, 1991.

SHI T AND APKARIAN AV. Morphology of thalamocortical neurons projecting to the primary somatosensory cortex and their relationship to spinothalamic terminals in the squirrel monkey. *J Comp Neurol* 361: 1–4, 1995.

SHI T, STEVENS RT, TESSIER J, AND APKARIAN AV. Spinothalamocortical inputs nonpreferentially innervate the superficial and deep cortical layers of SI. *Neurosci Lett* 160: 209–213, 1993.

SHOLL DA. *The Organization of the Cerebral Cortex*. New York: Wiley, 1956.

SHOLL DA AND UTTLEY AM. Pattern discrimination and the visual cortex. *Nature* 171: 387–388, 1953.

SILLITTO AM, JONES HE, AND GERSTEIN GL. Feature-linked synchronization of thalamic relay cell firing induced by feedback from the visual cortex. *Nature* 369: 479–482, 1994.

SINGER W AND GRAY CM. Visual feature integration and the temporal correlation hypothesis. *Annu Rev Neurosci* 18: 555–586, 1995.

STERIADE M. Coherent oscillations and short-term plasticity in corticothalamic networks. *Trends Neurosci* 22: 337–345, 1999.

SZENTAGOTHAI J AND ARBIB MA. *Conceptual Models of Neural Organization*. Cambridge, MA: MIT Press, 1975.

TURNER JP, ANDERSON CM, WILLIAMS SR, AND CRUNELLI V. Morphology and membrane properties of neurones in the cat ventrobasal thalamus in vitro. *J Physiol (Lond)* 505: 707–726, 1997.

VAADIA E, HAALMAN I, ABELES M, BERGMAN H, PRUT Y, SLOVIN H, AND AERTSEN A. Dynamics of neuronal interactions in monkey cortex in relation to behavioral events. *Nature* 373: 515–518, 1995.

WILLIAMS SR, TURNER JP, ANDERSON CM, AND CRUNELLI V. Electrophysiological and morphological properties of interneurones in the rat dorsal lateral geniculate nucleus in vitro. *J Physiol (Lond)* 490: 129–147, 1996.

WILLIS WD JR. *The Pain System*. New York: Karger, 1985.

WILSON MA AND MCNAUGHTON BL. Dynamics of the hippocampal ensemble code for space. *Science* 261: 1055–1058, 1993.